Electrical Power and Energy Systems 130 (2021) 106763

Contents lists available at ScienceDirect

International Journal of Electrical Power and Energy Systems

journal homepage: www.elsevier.com/locate/ijepes

A two-level over-voltage control strategy in distribution networks with high PV penetration

Mohammadreza Emarati [a], Mostafa Barani [a], Hossein Farahmand [a,*], Jamshid Aghaei [b], Pedro Crespo del Granado [c]

[a] Department of Electric Power Engineering, Norwegian University of Science and Technology (NTNU), Trondheim NO-7491, Norway
[b] LUT School of Energy Systems, Lappeenranta–Lahti University of Technology (LUT), Yliopistonkatu 34, 53850 Lappeenranta, Finland
[c] Department of Industrial Economics and Technology Management, Norwegian University of Science and Technology (NTNU), Trondheim NO-7491, Norway

ARTICLE INFO

Keywords:
Over-voltage control strategy
On-load tap changer
Battery energy storage systems
Network partitioning
Variable renewable energy sources
Smart distribution network
System flexibility

ABSTRACT

Over-voltage in low voltage feeders due to the increasing penetration level of photovoltaic (PV) is a crucial issue to be addressed. There is a need to use more advanced voltage control methods to satisfy the response time of the control system. In this paper, a two-level voltage control strategy is presented. In the first level, based on day-ahead PV production scenario, Both the on-load tap changer (OLTC) and the battery energy storage systems (ESSs) are applied to deal with over-voltage in the peak of PV generation and as well the voltage drop in the peak of demand. In this level, the batteries and the tap position of the feeder transformer are optimally set in order to improve the voltage profile for the entire planning horizon (next day) taking into account the uncertainties in the PV production. In the second level, based on the partitioning of the distribution network, reactive power compensation capability of PV inverters is employed to fine-tune the voltage profile for the next operating hour. To model the uncertainty pertaining to the output power of PV units, the parameters of beta distribution function are estimated for each hour time interval, and then Monte Carlo simulation method is used to generate daily scenarios. In order to reduce the complexities and computational burden, the linearized model of power flow equations and PV inverters have been implemented. A real and practical, 10 kV, 37-bus system is used to test the performance of the proposed method.

1. Introduction

In recent years, awareness about the environmental impacts of fossil fuel-based power generation and decrease in photovoltaic (PV) panel prices, promotes the consumers to prosumers with decentralised generation into the distribution grids [1,2]. Moreover, technical advancements and socially acceptable cost of the PV systems stimulate rapid growth in installed residential solar generating capacity around the world [3]. By increasing the penetration level of renewable energy sources and connecting new PV systems to the grid, new challenges will arise in the distribution networks [4]. These challenges are related to power quality aspects [5] such as voltage regulation [6], voltage rise [7], voltage unbalancing [8] and transmission lines overloading [9].

Voltage increases during peak solar generation times due to higher amounts of reverse power flow. This over-voltage is one of the critical factors, which limits the amount of PV systems installed in the grid [10]. Applying appropriate voltage control methods creates incentives to find opportunities for installing new PV systems to the grid. Therefore, advanced voltage control methods are required to ensure reliable operation of the distribution grids.

Conventionally, the distribution system operator (DSO) applies different voltage control devices such as on-load tap-changing transformers [7], static var compensators (SVC) [11], step voltage regulator (SVR) [12] and shunt capacitor (SC) [13] to control the voltage profile. By employing the real and reactive power control capabilities of the PV inverters, active power compensation(APC) [14] and reactive power compensation (RPC) [14,15], are two different methods to solve the over-voltage issue. Generally, to ensure that the voltage magnitude does not exceed the predefined limitations, a combination of these methods is used in a distribution grid [7].

To solve the over-voltage issue in the RPC method, the unoccupied capacity of the PV inverter is applied for reactive power compensation. This capability of the inverters makes the PV units similar to a controllable source. A centralized/decentralized approach is considered

* Corresponding author.
E-mail address: Hossein.farahmand@ntnu.no (H. Farahmand).

https://doi.org/10.1016/j.ijepes.2021.106763
Received 1 May 2020; Received in revised form 23 October 2020; Accepted 27 December 2020

in [2]. In this approach, the DSO finds the appropriate amounts of active/reactive power by dispatching and sends the obtained values to the local controllers through telecommunication links. In [16], a centralised control method is applied for voltage regulation at DSO level. The applied method consists of two layers. In the first layer, each grid-interfaced inverter is set locally based on a P(V) droop control strategy. Furthermore, the control voltage is performed in order to minimise the active power curtailment in the second layer, as a complement to the first layer.

A two-level volt/var control scheme for PV aggregators is presented in [17]. At the lower level, the rooftop PV inverters are aggregated through the consensus algorithm, and the droop controllers set the reactive power output of each PV inverter. At the higher level, to minimize the power loss, the reactive power of the PV inverters is dispatched. The distributed structure of this approach increases the system resilience. In [18], a similar three-level approach is introduced by the same research team and validated by applying the power hardware-in-the-loop (PHIL) experiment.

In [19], control and coordination of OLTC and RPC capabilities for voltage regulation in the distribution systems are proposed. In this approach, the authors used mode estimation of OLTC control, as well as capacity, location and power factor limits of inverters to mitigate an over-voltage at a remote bus on the same feeder.

Another solution to an over-voltage problem is to use ESSs, e.g., battery storage systems, in order to store the energy instead of curtailing PV units [20,21]. These systems can have a vital role in maintaining the voltage profile within the acceptable range. To deal with the over-voltage problem, the battery charges in high PV generation periods and discharges in the other time-periods of the day. Different local voltage control strategies based on the coordinated use of PV and battery storage systems is presented in [22]. In this article, a droop-based control for batteries is considered in each house. Furthermore, the reactive power absorption capability of inverters is utilized to overcome over-voltage issues in some residential feeders. In order to regulate voltage profile, a real-time framework to coordinate PV inverters and batteries is provided in [23]. The proposed model is implemented in a weak distribution network with a high PV penetration. This method has a positive impact on the grid utility by decreasing line losses and supporting the peak load. Based on the cooperation of ESSs, a distributed voltage regulation approach is developed in [24] for high PV penetrated distribution networks. In this approach, each ESS is deemed as an individual agent who communicates with its nearby agents to make its own control decisions and at the same time improves the operational condition of the system.

A coordinated operation of ESSs and OLTC has been applied to voltage regulation of the distribution networks in recent literature. In [25], a coordinated strategy for optimal operation of ESSs and OLTC is applied. In this approach, ESS units play an active role in voltage regulation in addition to OLTCs to ensure the voltage quality. Moreover, in [26], a two-stage robust optimisation model is proposed for OLTC coordination with RPC and charge/discharge rates of ESSs.

The coordination of RPC methods and scheduling of the batteries is demonstrated as a suitable strategy to achieve an enhanced voltage profile [27]. However, the approaches, which consider the distribution grids are generally computationally heavy and applying these methods to the large systems is a difficult task. Therefore, because of the distributed nature of PV systems in the grid, using decentralized voltage control methods is a convenient alternative way to manage the voltage profile of the distribution network. A decentralized method for voltage regulation, and at the same time, reactive power dispatch is proposed in [28]. In this strategy, the control capability of fast response PV inverters is used to deal with voltage fluctuations.

Network partitioning methods with different objectives and characteristics have been introduced in [29–33]. In [34] a modularity index is introduced to apply for a partition detection algorithm. The especial advantage of this algorithm is that there is no need to initialize the number of partitions. In other words, the algorithm finds the optimal number of partitions by itself. In [30], an improved modularity index is introduced based on community detection algorithm to obtain the optimal network partitions. Accordingly, a complex problem is decomposed into several sub-problems, which can be solved using decentralized methods. Also, a two-step procedure for the optimal partitioning of smart distribution systems is demonstrated in [31]. In this approach, at first the optimal place of DG units is determined and then by applying a placement strategy to find the optimal situation of reclosers and batteries, the maximum supply adequacy in each partition is guaranteed. A robust voltage/var control approach for active distribution networks is presented in [35]. This method coordinates OLTC, capacitor banks and inverters with the aim of minimizing the power loss. To improve the quality of the algorithm, a clustering method is employed to reduce the amount of data exchanged between the adjacent partitions.

Although previously mentioned voltage control strategies are commonly used in the power system, applying some of these strategies in local areas and low-voltage grids are hard to be achieved. Moreover, the local over-voltage problems are observed in the distribution systems with high penetration of distributed solar generation and prosumers, e.g., in the German system [36,37]. In this article, a coordinated voltage control strategy to solve the local over-voltage problems with local control devices such as OLTC, batteries and RPC capability of the PV inverters is proposed.

A stochastic two-level control approach is presented for regulating the voltage profile in distribution networks with high PV penetration. In the first level, the Monte Carlo simulation is applied to model the uncertainty of PV production. Based on the generated scenarios, the optimal decisions on the tap position of the transformer in the reference bus and the operation of batteries for the next 24 time-periods, are made. In this level, the batteries are scheduled to mitigate the effects of PV generations on the voltage rise of the grid. Next, in the second level, the voltage profile is restored to the acceptable range by using RPC capability of PV inverters during the time-periods, which there is an over-voltage because of high PV penetration. It should be mentioned that this is implemented in the distribution grid that is divided into multiple smaller partitions. Thus, by selecting the most critical partitions in the grid, only the inverters in these partitions take a role in RPC process. Moreover, in peak load periods by consuming more active power, there will be a drop in voltage magnitude. In this case, inverters are able to help the grid to avoid voltage drop by injecting reactive power.

The main contributions of this article fall under the following items:

1. A stochastic two-level voltage control strategy is proposed based on taking advantages of battery energy storage systems as well as RPC capability of inverters to regulate the voltage magnitude in addition to the optimal decisions on the tap position of OLTC. The uncertainty of PV production is taken into account in the first level of the proposed voltage control strategy, while the operational condition of the grid is considered using the AC optimal power flow.
2. A network partition-based zonal voltage control scheme is considered in the second level of the proposed voltage control strategy.
3. Linear formulations are considered for both power flow and the AC inverter. Therefore, the voltage control strategy addressed in this paper is formulated as a linear optimisation problem at each level. Consequently, CPLEX, as a high-performance solver, is adopted for modelling and solving these models.

In Table 1, the proposed method is compared with the approaches recently presented in the literature. In the first column of this table, the voltage control methods are divided into two categories: centralized and decentralized. In the centralized method, the voltage regulation is done through a central coordinator using system communication devices such as OLTC and voltage regulator. However, in decentralized methods, voltage control is done locally through an active manner with less

Table 1
Taxonomy of the recent works in the area.

Ref.	Coordination scheme	Levelized Optimization	Utilizing			Network Partitioning	Power Flow	Time Scale	Objective
			APC	RPC	ESS				
[14]	Decentralized	No	No	Yes	No	No	–	Sec	Local voltage regulation
[17]	Centralized	Two level	No	Yes	No	No	AC	Sec	Utilize PV inverters for voltage regulation
[25]	Decentralized	No	No	No	Yes	Yes	–	Hour	Enhance the impact of ESS on voltage regulation
[26]	Decentralized	Two stage	Yes	Yes	Yes	No	Branch flow	Hour	Minimization of the cost in the main grid
[35]	Centralized	Two stage	Yes	No	No	Yes	AC	–	Minimization of power loss
[20]	Decentralized	No	No	Yes	Yes	No	–	Hour	Voltage regulation in low voltage networks
[22]	Decentralized	No	Yes	Yes	Yes	No	–	Minute	Voltage control through self-consumption strategies
[18]	Decentralized/ Centralized	Three level	No	Yes	No	No	AC	Sec	Voltage regulation through inverter capabilities
[21]	Decentralized/ Centralized	No	No	No	Yes	No	AC	Hour	Voltage regulation through ESS coordination
[23]	Decentralized	No	No	No	Yes	No	–	Sec/ Hour	Coordination of PV inverters and ESSs for voltage regulation
[24]	Decentralized/ Centralized	No	No	No	Yes	No	–	Minute	Voltage regulation through cooperative manner of ESSs
Pro.*]	Decentralized/ Centralized	Two level	No	Yes	Yes	Yes	Linear	Hour	Over-voltage control through ESS scheduling and RPC

* Proposed method.

number of communication devices. In light-load mode, the battery works as an auxiliary service, with less emphasis on active power injection into the network. So, as it shown in Fig. 2 (b) the power exchange between DGs and the grid is limited in a predefined range. The lines l_5 to l_{10} in this figure describe the operational constraints for the inverter in light-load conditions.

2. Model description

The proposed voltage control method in this article consists of two-levels. In the first level, the OLTC in the reference bus and the batteries, which are considered in PV buses are scheduled for the 24 h of the planning period. Then, in the second level, the voltage is restored to the acceptable range using hourly reactive power control capability of inverters. Note that, the objective functions of both optimisation problems are to minimize the deviation of the voltages from 1 p.u. However, in the first level, the decision variables are the tap position of the OLTC and the charge and discharge power of the batteries. The optimal values of these decision variables will be considered as inputs to the second level of the proposed voltage control strategy. Moreover, in the second level the decision variables are the injected amount of reactive power taken from the inverter of each PV bus.

The subsequent section describes the modelling of different components in the proposed voltage control strategy.

2.1. Bus considerations

The interface between the distribution feeder and the three-phase inverter is depicted in Fig. 1. As illustrated in this figure, battery, PV, and local load have been considered as potential components connected, at a typical bus. Moreover, it can be seen that in different situations, the active and reactive power can flow alternatively in both directions. Because of feeder impedance, there is a voltage drop in the direction of power flow. For each bus i, scenario ω and time-period t, the voltage difference between the point of common coupling (PCC) voltage and the bus voltage ($\Delta V_{i,\omega,t}$) can be written as [38]:

$$\Delta V_{i,\omega,t} \approx \frac{R_i P_{i,\omega,t} + X_i Q_{i,\omega,t}}{V^*_{i,\omega,t}} \qquad \forall i, \forall \omega, \forall t \tag{1}$$

where $R_i + jX_i$ represent the impedance of the line which connects the bus i to the grid. $P_{i,\omega,t}$ and $Q_{i,\omega,t}$ are net active and reactive power at the bus i, scenario ω and the time-period t, respectively. Also, $V_{i,\omega}$ can be considered as the reference voltage:

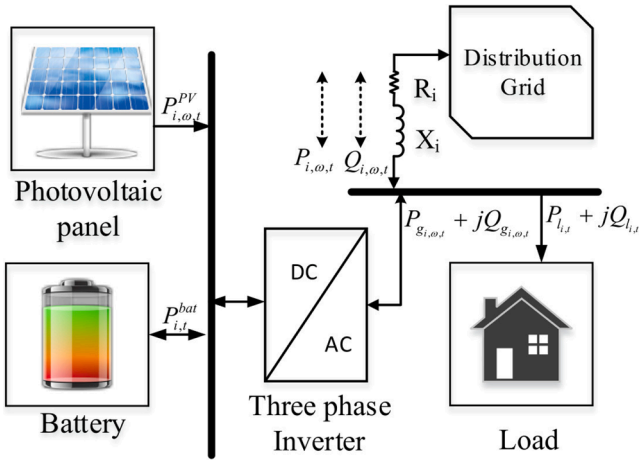

Fig. 1. A typical bus with PV and battery.

$$\Delta V_{i,\omega,t} \approx R_i P_{i,\omega,t} + X_i Q_{i,\omega,t} \qquad \forall i, \forall \omega, \forall t \tag{2}$$

Here, $P_{i,\omega,t}$ and $Q_{i,\omega,t}$ are achieved by

$$P_{i,\omega,t} = P_{g_{i,\omega,t}} - P_{l_{i,t}} \qquad \forall i, \forall \omega, \forall t \tag{3}$$

$$Q_{i,\omega,t} = \pm Q_{g_{i\omega t}} - Q_{l_{i,t}} \qquad \forall i, \forall \omega, \forall t \tag{4}$$

where $P_{g_{i,\omega,t}}$ and $Q_{g_{i,\omega,t}}$ are active and reactive generated power at the bus i, scenario ω and the time-period t, respectively; $P_{l_{i,t}}$ and $Q_{l_{i,t}}$ are active and reactive load at the bus i and at the time-period t, respectively. Consequently, active and reactive power can be used to control voltage. Also, different scenarios of injected power can impact the voltage profile. For instance, during the day time when DGs produce active power the voltage in different buses rises. Note that, the most important purpose for solar power plant owners is to maximize their active power injection. Whereas, in this study, the main objective is to improve the voltage profile in distribution grids in light of maximizing injected power by DGs to maintain the voltage within safe operating range.

2.2. Objective function equation

The objective function in the first and second levels of the proposed voltage control strategy is the same and considered as follows, leading to minimize the voltage deviation around one per unit:

$$\text{Objective function}: \ \min\left(\sum_{i=1}^{N_I}\sum_{\omega=1}^{N_\Omega}\sum_{t=1}^{N_T}\pi_\omega.\left|V_{i,\omega,t}-1\right|\right) \tag{5}$$

where π_ω is the probability of occurrence for each scenario, $V_{i,\omega,t}$ is the magnitude of the voltage for the bus i (in per unit), scenario ω and at the time-period t. N_I, N_ω and N_T are the number of PQ buses, number of scenarios and the time horizon, respectively. Eq. (5) is nonlinear due to the presence of the absolute value function. Thus, by applying an auxiliary variable $y_{i,\omega,t}$, this equation can be transformed into a linear equation:

$$\min \sum_{i=1}^{N_I}\sum_{\omega=1}^{N_\Omega}\sum_{t=1}^{N_T}\pi_\omega.y_{i,\omega,t} \tag{6}$$

Subject to

$$y_{i,\omega,t}\geqslant V_{i,\omega,t}-1 \quad \forall i,\forall\omega,\ \forall t \tag{7}$$

$$y_{i,\omega,t}\geqslant 1-V_{i,\omega,t} \quad \forall i,\forall\omega,\ \forall t \tag{8}$$

$$y_{i,\omega,t}\geqslant 0 \quad \forall i,\forall\omega,\ \forall t \tag{9}$$

2.3. Bus voltage constraints

The voltage of buses should be considered within a permitted range:

$$V^{\min}\leqslant V_{i,\omega,t}\leqslant V^{\max} \quad \forall i,\forall\omega,\ \forall t \tag{10}$$

In this relation, $V^{\min}$ and $V^{\max}$ are minimum and maximum allowed values of voltage in each bus, respectively.

2.4. OLTC constraints

The voltage magnitude at the reference bus is considered as a function of OLTC tap position:

$$V_{\text{ref,t}}=1+\left(tp_t\times\frac{V^{\max}-V^{\min}}{tp^{\max}-tp^{\min}}\right) \quad \forall t \tag{11}$$

$$tp^{\min}\leqslant tp_t\leqslant tp^{\max} \quad \forall t \tag{12}$$

where tp_t is an integer variable denoting the tap position, $tp^{\min}$ and $tp^{\max}$ are minimum and maximum values for tap position, respectively. Note that, $tp^{\min}$ and $tp^{\max}$ are considered to be -8 and $+8$, respectively.

2.5. Power flow equations

Eqs. (13) and (14) characterize the constraints of the load flow (active and reactive power balance at each bus) in the distribution grid, as:

$$P_{i,\omega,t}=\sum_{\substack{j=1\\ j\neq i}}^{N_I}V_{i,\omega,t}V_{j,\omega,t}Y_{ij}\cos(\delta_{i,\omega,t}-\delta_{j,\omega,t}-\theta_{ij}) \quad \forall i,\forall\omega,\forall t \tag{13}$$

$$Q_{i,\omega,t}=\sum_{\substack{j=1\\ j\neq i}}^{N_I}V_{i,\omega,t}V_{j,\omega,t}Y_{ij}\sin(\delta_{i,\omega,t}-\delta_{j,\omega,t}-\theta_{ij}) \quad \forall i,\forall\omega,\forall t \tag{14}$$

where, $\delta_{i,\omega,t}$ and $\delta_{j,\omega,t}$ are angles of voltage at buses i and j and scenario ω and time t, respectively; Y_{ij} and θ_{ij} are the magnitudes in per unit and angle of the admittance of branch between bus i and j, respectively. These load flow equations are nonlinear. Nonlinearity increases computational complexity and may cause convergence problems. Here, to avoid this problem, a linearized version of load flow is considered. In a per unit system, the magnitudes and angles of the bus voltages are around 1 and 0, respectively. Consequently, the load flow equations are linearized around this point using Eqs. (15) and (16), respectively [39].

$$P_{i,\omega,t}=Y_{ij}\sum_{\substack{j=1,j\neq i}}^{N_I}[\cos\theta_{ij}+\cos\theta_{ij}{}^*(V_{i,\omega,t}-1)+\cos\theta_{ij}{}^*(V_{j,\omega,t}-1) -\sin\theta_{ij}{}^*(\delta_{j,\omega,t})+\sin\theta_{ij}{}^*(\delta_{i,\omega,t})] \quad \forall i,\forall\omega,\forall t \tag{15}$$

$$Q_{i,\omega,t}=Y_{ij}\sum_{\substack{j=1,j\neq i}}^{N_I}[\cos\theta_{ij}(\delta_{i,\omega,t})-\cos\theta_{ij}{}^*(\delta_{j,\omega,t})-\sin\theta_{ij} -\sin\theta_{ij}{}^*(V_{i,\omega,t}-1)-\sin\theta_{ij}{}^*(V_{j,\omega,t}-1)] \quad \forall i,\forall\omega,\forall t \tag{16}$$

2.6. Battery equations

Management of charging and discharging of the batteries is strongly required to be considered. Thus, Eqs. (17) and (18) are applied to manage and control the operation of the batteries. The below equations show the relation between the state of charge (SoC) of the battery and its previous value with respect to the charge and discharge power at time t:

$$SoC_{i,t}=SoC_{i,t-1}+P_{i,t}^{\text{ch}}{}^*\eta_c-\frac{P_{i,t}^{\text{dch}}}{\eta_d} \quad \forall i,\forall t \tag{17}$$

$$P_{i,t}^{\text{bat}}=P_{i,t}^{\text{dch}}-P_{i,t}^{\text{ch}} \quad \forall i,\forall t \tag{18}$$

where $SoC_{i,t}$ denotes the state of charge of the battery in the bus i at the time-period t, $P_{i,t}^{\text{bat}}, P_{i,t}^{\text{ch}}$ and $P_{i,t}^{\text{dch}}$ are the net injected, input and output power of the battery in the bus i at the time-period t. The parameters η_c and η_d are the charge and discharge efficiency of the battery, respectively. The charge and discharge rates of the battery in the bus i are limited as follows:

$$0\leqslant P_{i,t}^{\text{ch}}\leqslant x_{i,t}P_i^{\text{ch,max}} \quad \forall i,\forall t \tag{19}$$

$$0\leqslant P_{i,t}^{\text{dch}}\leqslant (1-x_{i,t})P_i^{\text{dch,max}} \quad \forall i,\forall t \tag{20}$$

where the binary variable $x_{i,t}$ represents the charge or discharge state of the battery at the time-period t. If the battery is charged $x_{i,t}=1$ and $x_{i,t}=0$ if the battery is discharged. $P_i^{\text{ch,max}}$ and $P_i^{\text{dch,max}}$ are the maximum allowed values of charge and discharge, respectively. Moreover, aiming at preventing damages to the battery, Eq. (21) limits the SoC of the battery. Therefore, the SoC of the battery is controlled in a way that it doesn't exceed the predefined limitations:

$$SoC^{\min}\leqslant SoC_{i,t}\leqslant SoC^{\max} \quad \forall i,\forall t \tag{21}$$

where $SoC^{\min}$ and $SoC^{\max}$ are minimum and maximum amounts of allowed state of charge, respectively.

In this article, we consider battery in all PV buses. Therefore, the active power generation value in these buses is obtained through Eq. (22).

$$P_{g_{i,\omega,t}}=P_{i,\omega,t}^{\text{PV}}+P_{i,t}^{\text{bat}} \quad \forall\omega,\forall i,\forall t \tag{22}$$

where $P_{g_{i,\omega,t}}$ is the amount of active power generation in the bus i at the time-period t and scenario ω. Furthermore, $P_{i,\omega,t}^{\text{PV}}$ is the active power generation of PV installed in bus i, scenario ω and at the time-period t. The value of $P_{i,t}^{\text{bat}}$ is positive when the battery is discharging and its negative when the battery is charging.

Finally, the state of charge of the battery must be equal at the start and the end of the day [31,40]:

$$SoC_{i,\omega,t} = SoC^{\text{Init}} \quad \forall i, \forall \omega, t = T \tag{23}$$

where SoC^{Init} is a parameter, which shows the initial state of charge of the battery.

The optimized level of active power exchange between the battery and the grid is achieved by considering these constraints.

2.7. Inverter equations

As it is illustrated in Fig. 1 the photovoltaic panels and the battery are connected to the grid by a three-phase inverter. The inverter can control the amount of injected or absorbed active and reactive power. Consequently, the inverter has a capability curve similar to synchronous generators to control terminal voltage by regulating the amount of reactive power compensation. The capability power curve is introduced to limit the active and reactive power:

$$S_{\text{inv}_{i,\omega,t}} = \sqrt{P^2_{g_{i,\omega,t}} + Q^2_{g_{i,\omega,t}}} \quad \forall i, \forall \omega, \forall t \tag{24}$$

where $S_{\text{inv}_{i,\omega,t}}, P_{g_{i,\omega,t}}$ and $Q_{g_{i,\omega,t}}$ are the apparent, active and reactive power generation of the inverter, respectively. Thus, the reactive power is limited by the active power that it is supposed to deliver. Since Eq. (24) is nonlinear, it can be linearized using the following procedure. As it's displayed in Fig. 2, based on the hourly loading within the day, the time-periods are categorized into two parts: heavy and light load periods.

In heavy load hours, active power is injected from the DG side to the network. Therefore, the power factor of the inverter is limited to a lead-lag range which is close to 1. This limitation is considered based on common standards and local regulations. More detailed information about these equations is described in the appendix. In this way, as shown in Fig. 2(a), the following constraints are expressed for heavy load conditions:

$$l_m(PV, t_{\text{Heavy}}) \leqslant 0 \quad \forall m \in \{1,2,3,4\} \tag{25}$$

wherein this equation l_m indicates line number m, PV and t_{Heavy} specifies the nodes with PV installation and the time-periods with a heavy load, respectively.

In the light load mode, the reactive power generation of the inverter helps to improve the voltage profile of the grid. In light load hours, the inverter is allowed to operate with lower values of power factor. As shown in Fig. 2(b), in this case the following constraints can be considered for the light load mode:

$$l_m(PV, t_{\text{Light}}) \leqslant 0 \quad \forall m \in \{5,7,9\} \tag{26}$$

$$l_m(PV, t_{\text{Light}}) \geqslant 0 \quad \forall m \in \{6,8,10\} \tag{27}$$

where t_{Light} indicates light load time-periods.

In addition, changes of reactive power amount in PV nodes are controlled by Eqs. (28) and (29).

$$-Q_i^{\text{absorb}} \leqslant \Delta Q_{i,\omega,t} \leqslant Q_i^{\text{absorb}} \quad i \in PV, \forall \omega, \forall t \tag{28}$$

$$-\cos^{-1}(0.9) \leqslant \varphi_{i,\omega,t} \leqslant \cos^{-1}(0.9) \quad i \in PV, \forall \omega, \forall t \tag{29}$$

$\Delta Q_{i,\omega,t}$ is the amount of changes in reactive power in each PV node; Q_i^{absorb} is the maximum amount of reactive power absorption capacity in node i. $\varphi_{i,\omega,t}$ is the power factor angle of inverter for bus i, scenario ω and the time-period t.

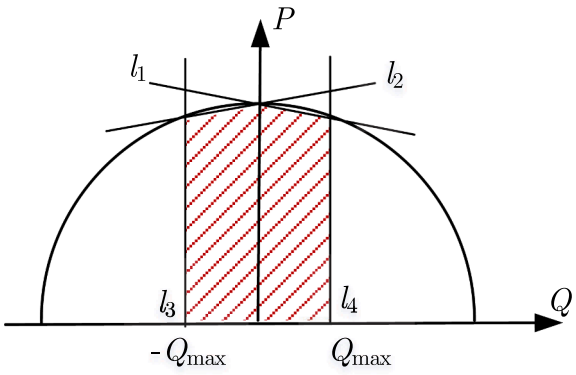

(a) a

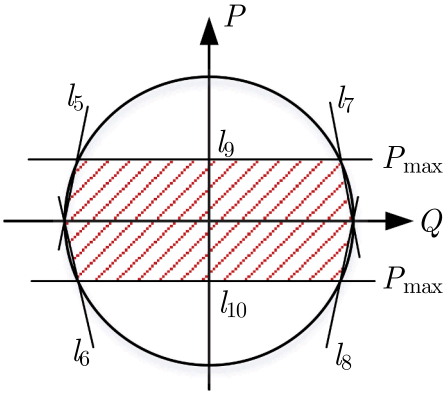

(b) b

Fig. 2. Linear inverter capability curve: (a) heavy load, (b) light load mode.

3. The proposed voltage control strategy

This section describes the proposed two-level voltage control strategy. In the first level of the proposed strategy, the best tap position for the OLTC in the reference bus and the day-ahead schedule of batteries are obtained by considering the uncertainty of PV production. Accordingly, by implementing the generated PV production scenarios, the optimal charge and discharge rates of the batteries for each hour of the next day will be characterized. Moreover, in the second level, based on the previous settings for the batteries and OLTC, the hourly amount of reactive power compensation for most critical partitions are determined. In the following subsections, we explain details of each level in the proposed voltage control strategy.

3.1. First level: OLTC adjustment and daily scheduling of batteries

One of the most important advantages of battery is its ability to control the rate of active power injection to the grid. In other words, storing the energy in the battery and injection of it at the right time leads to a more stable voltage profile for the grid.

In a typical sunny day, due to extensive production of PVs combined with a light load, the voltage value increases. In this condition, if the voltage exceeds its allowed range, even if there is a lot of PV production, some parts or all of production needs to be curtailed. Therefore, utilizing batteries and ESSs efficiently helps to improve the voltage profile. In other words, the battery can act as a buffer to charge and discharge during the time-periods of solar peak generation and during the night, respectively.

In the first level of the proposed voltage control strategy, the tap position of OLTC in the reference bus and the optimal operation of batteries during the next 24 time perids are scheduled. In this way, the charge and discharge rates for each battery at each period is specified to

improve the voltage profile. The objective function of this problem is considered as Eq. (5). Therefore, batteries are scheduled in a manner that the voltage profile maintains close to 1 p.u value. Here, the decision variables include: an integer variable, which determines the tap position in the reference bus at each time interval, a binary variable, which specifies the charging or discharging of the battery for each PV bus at each time interval, and the amount of active power exchange between the battery and the grid.

The optimisation problem in this level can be expressed as the following model:

Daily scheduling of batteries: Objecting function:(6).

Subject to: Eqs. (3), (4), (7)–(9), (11), (12), (15)–(23).

In ordinary conditions, the OLTC in the reference bus helps to maintain the voltage profile within its allowed range. However, in the peak PV generation of some scenarios, the OLTC alone is not capable of keeping the voltage in its allowed range. In this condition, optimal scheduling of the existing batteries helps the grid to experience an improved voltage profile. Yet, still in some hours of the day due to high excess amount of PV production, this level is not sufficient and the voltage value exceeds the acceptable range.

Characterization of PV production uncertainty: The amount of PV production is a stochastic parameter, which is mostly related to weather condition. By considering the uncertainty for PV production, the results of the proposed method get closer to real situations. In this paper, the Monte Carlo simulation method [41] is applied to generate PV production scenarios. For this propose, in the first level of the proposed method, the parameters for the Beta distribution function are estimated using the historical solar generation data. The PV production scenarios are produced by employing the estimated beta distribution functions. In the next step, the number of scenarios is reduced to a specific number, to decrease the computational burden of the proposed model while providing a good approximation of the PV units. Here, a fast-forward scenario reduction method [42] is used to reduce the number of scenarios. Therefore, the first level of the proposed method determines the daily charge and discharge rates of the batteries based on the final set of scenarios and their corresponding probability of occurrence.

3.2. Second level: reactive power compensation

In the second level, based on the partitioning of the distribution network, reactive power compensation capability of PV inverters is employed to fine-tune the voltage profile for the next hour.

According to the IEEE Std 1547.4, large distribution systems can be partitioned into a number of microgrids to facilitate powerful control and operational infrastructure in the future distribution systems [43]. It is due to the existing complexity of the system hosting large capacity of renewable energy resources.

Network partitioning

The operation of the distribution networks becomes more complicated by adding distributed PVs to these systems. In a large network, the control of all PVs using a centralized method is quite difficult. Therefore, for voltage control issues, it is reasonable to cluster buses with common features in the same partition. Here, the objective of the network partitioning is to control the zonal voltage in a shorter time using the minimum amount of reactive power. Moreover, by applying the network partitioning, the number of optimisation variables and control dimension is significantly reduced. The proposed network partitioning is conducted based on the topology of the network.

In our algorithm, we allocate the inverters with similar reactive power control capabilities in the same partition. Consequently, buses, which are existing in the same partition, are more coupled with each other compared with the buses in the other partitions. In [34], by introducing a modularity index (ρ), a community detection algorithm for partitioning complex networks is presented. We use the similar approach in the proposed voltage control strategy to find the optimum adjacent partition provided that the reactive power capability of inverters within a given partition is not enough to bring the voltage back to the permissible variation range. The Eq. (30) determines the value of the modularity index [30,34]:

$$\rho = \frac{1}{2M}\sum_i\sum_j\left[A_{ij} - \frac{k_i k_j}{2M}\right]\psi_{ij} \tag{30}$$

where A is the adjacency matrix, which denotes the weighted value of the edges between nodes i and j. If two nodes are linked together $A_{ij} = 1$, otherwise $A_{ij} = 0$. The variable e is determined by $M = \frac{1}{2}\sum_i\sum_j A_{ij}$, which is total edge weight. $k_i = \sum_j A_{ij}$ is the sum of all weighted values of adjacency matrix connected to the bus i; and the value of $\psi_{ij} = 1$ if nodes i and j are selected to be in the same partition, otherwise $\psi_{ij} = 0$. The pseudo-code for the applied network partitioning method is shown in Algorithm 1.

By applying zonal based reactive power control capability of the inverters in each hour, the optimal value of necessary reactive power in most critical partitions is determined to experience the optimized voltage profile.

Algorithm 1. Network partitioning

```
Initialize: N//number of buses, A//initial adjacency matrix, P// number of final partitions
while N > P
    Calculate matrices e, k, δ
    Calculate ρ matrix using Eq. (30)
    for each bus i do
        Find the most adjacent node to node i (node k)
        Consider node i and k as one new node
        N←N−1
        if The node j is not selected before then
            Consider the node i as a separate partition
        Create new adjacency matrix A_new
    A←A_new
```

Second level process

After applying the mentioned network partitioning method, a distribution network can be divided into N separated partitions. In this case, the overall distribution network is presented by a set of partitions$\{P_1, P_2, \ldots, P_k, \ldots, P_N\}$. Here, since the different partitions are separated in an optimal way, the proposed process of voltage control can be applied to each partition separately. In general, two types of buses in each partition are considered: PV buses and normal buses, which don't have voltage control capability.

As mentioned before, the amount of absorption or injection of reactive power in PV buses is regulated by the inverter capability. In the second level of the proposed voltage control strategy, the optimal values of these variables are determined by solving the following optimisation problem.

Zonal voltage control by reactive power absorption:

Objective function: (6).

Subject to: Eqs. (3), (4), (7)–(10), (15)–(29).

After considering and scheduling the batteries in the first level of the proposed voltage control strategy, as shown in Fig. 3, in the second level, at first, the load flow analysis will be performed. If an over-voltage is observed at each bus, the amounts of active and reactive power in each node and therefore the power factor of the connected inverter to the given bus will be obtained. In the second step, the most critical partition, which has the bus with a maximum over-voltage will be identified. In the third step, the zonal voltage control strategy is carried out. The optimisation in this level is performed in GAMS software. The data will be transformed in a way that, only buses of the most critical partition have the ability to absorb reactive power. Afterwards, the overall load flow will be executed one more time, if still an over-voltage exists in the system, the mentioned procedure will be used again to absorb more reactive power from next critical partitions. This process is repeated again and again till there is no over-voltage in the system or we have

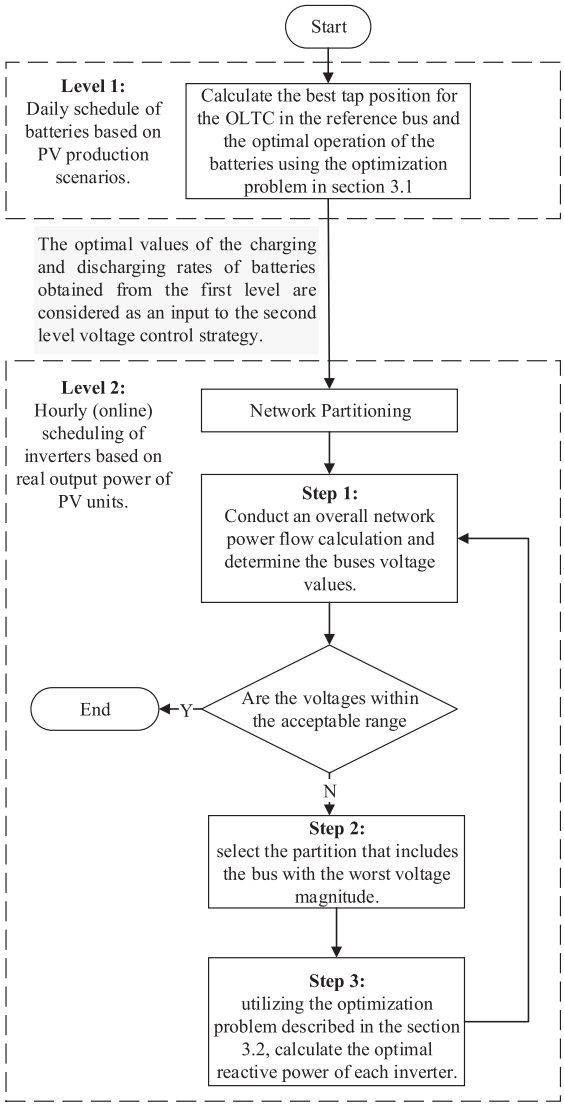

Fig. 3. Flowchart of the proposed two-level voltage control strategy.

used all capability of reactive power absorption in all partitions of the grid. It is worth to be mentioned that the proposed methodology in the second level can be implemented for online voltage control in distribution networks.

4. Simulation results

The 10 kV radial 37-bus feeder in [30] has been used for implementing and evaluation of the proposed two-level voltage control strategy. Fig. 4 indicates the structure of this feeder. The reference values for voltage and power is considered as 10 kV and 1 MVA, respectively. The permissible voltage variation range is assumed to be between 0.95 and 1.05 p.u. Bus number 1 is the reference bus with a transformer equipped with OLTC. This feeder does not experience overvoltage in its current condition. However, it is assumed that there is a plan for installing totally 18.315 MW PV to this system. The current installed values and its future values for each bus is shown in Fig. 5. Detailed information about the load, PV installation capacity and line data is available in [30].

In this article, we assumed that there is a battery in all PV buses. The capacity of the existing battery in each PV bus is considered as 20 percent of installed PV in that bus. The initial SoC of each battery is considered 45 percent. Moreover, the maximum charge and discharge rates of the battery is considered as 20 percent of the battery capacity. In order to make sure that there is enough reactive power support from inverters, generally, the capacity of inverters are considered sufficiently large enough to perform the simulations. The linear model for the inverter is implemented. Here, the capacity of inverters in each PV bus is considered 10 percent more than installed PV at the same bus. The operational power factor for all inverters is considered in the range of (−0.9 to 0.9).

Fig. 4 shows the results of applying the network partitioning method in Section 3 to the test system. According to Algorithm 1, at first, the algorithm considers each bus as a separate partition. Then the modularity index between every two nodes is calculated. Therefore, the buses with a higher amount of modularity index are selected to be inside one partition. Next, each new partition is assumed as one node and again, the algorithm calculates the modularity index for every two new nodes. After four consecutive repetitions, the partitions are formed as depicted in Fig. 4. In this figure, the border between partitions $\{P_1, P_2, \cdots, P_6\}$ are represented by a dashed line.

In order to generate scenarios for the output power of PV units, historical data of solar radiation is used. The solar radiation time series from the Reanalysis global weather model [44], are implemented for constructing synthetic solar time series. Reanalysis solar radiation data from the year 2005 to 2015 is provided for Spain with an hourly time resolution. The preparation of the solar radiation is based on the RDP-mapping (Reanalysis Data Points) at $2.5^\circ \times 2.5^\circ$ resolution. The annual data is applied to generate daily PV production scenarios.

The reduced set of scenarios, along with the expected PV generation and also the real PV generation for a specific day are depicted in Fig. 6. This real day is chosen in such a way that the maximum overvoltage is

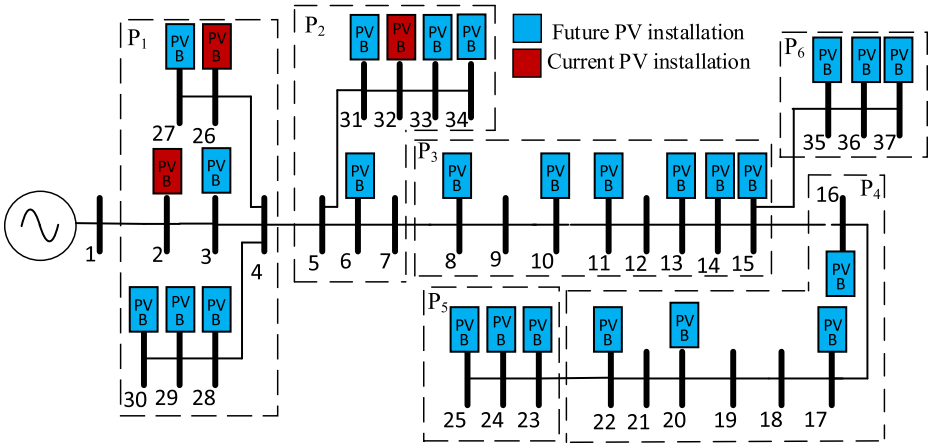

Fig. 4. The structure of 37-bus real distribution feeder under study.

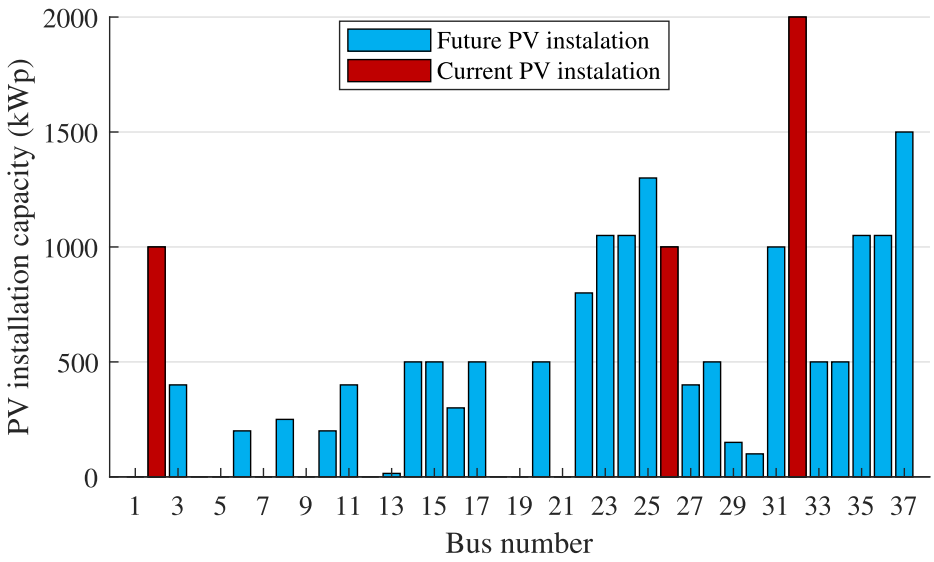

Fig. 5. Current and future PV installation capacity (kWp).

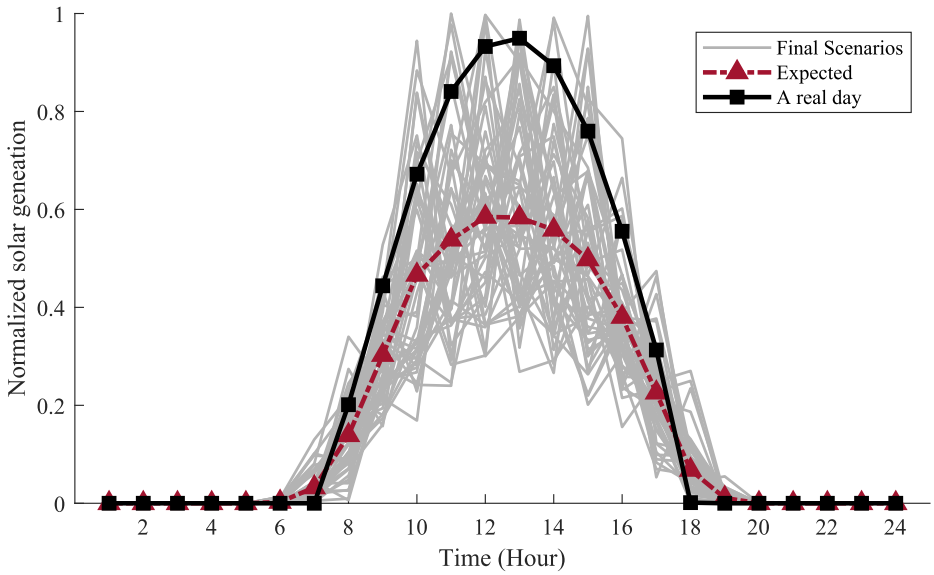

Fig. 6. Generated scenarios, Expected values and real PV production.

experienced at the peak of the solar generation. In other words, here, an attempt has been made to extend the results of the simulation to the worst-case scenario. As well, the considered per-unit load for the case study is illustrated in Fig. 7.

Fig. 8 depicts the voltage profile for the final set of scenarios in the first level of the proposed method. As can be seen in this figure, due to the diversity in the final set of PV production scenarios, the voltage profile has a wide range of variations. The voltage in the reference bus is set to 0.975 p.u. It should be mentioned that, in the first level of the proposed voltage control strategy, the tap position is set considering all possible scenarios. Furthermore, the expected voltage in the first level of the proposed strategy is illustrated by a red dashed line. This value is calculated, considering the probability of each PV production scenario.

The charge and discharge rates and also SoC of the battery in bus 35 is depicted in Fig. 9. As it is specified in this figure, using the first level of the proposed model (Section 3.1), the battery is scheduled in a way that it charges (negative values) in peak solar generation times and discharges (positive values) during the night hours. In other words, the SoC has it's minimum and maximum values at times 6 and 18 o'clock, respectively. This observation demonstrates that the batteries are organised in a way that they charge fully in PV production period. The reason why the battery is discharging in the last hours of the day is the constraint represented by Eq. (36), which forces the battery to have the same amount of SoC at points of start and the end of the day.

The obtained results of the first level, determine the tap position and the schedule of the batteries based on the expected PV production of the next day. Here, real data of PV production for a specific day in summer is selected to examine the performance of the second level. In other words, according to the obtained results of the first level, the amount of reactive power absorption for each partition will be specified.

As depicted in Fig. 6, for the selected day, the peak of PV generation occurs at hour 13. For this time-period, the performance of the second level of the proposed voltage control method is summarized as follows: Fig. 10 illustrates that by applying the first level of the proposed voltage control strategy, the voltage profile improves but it will not be kept within the permissible range. Since, bus 25 experiences the maximum amount of over-voltage, partition P_5 is selected for absorbing reactive power according to the first step in Fig. 3. The inverters of buses 23, 24

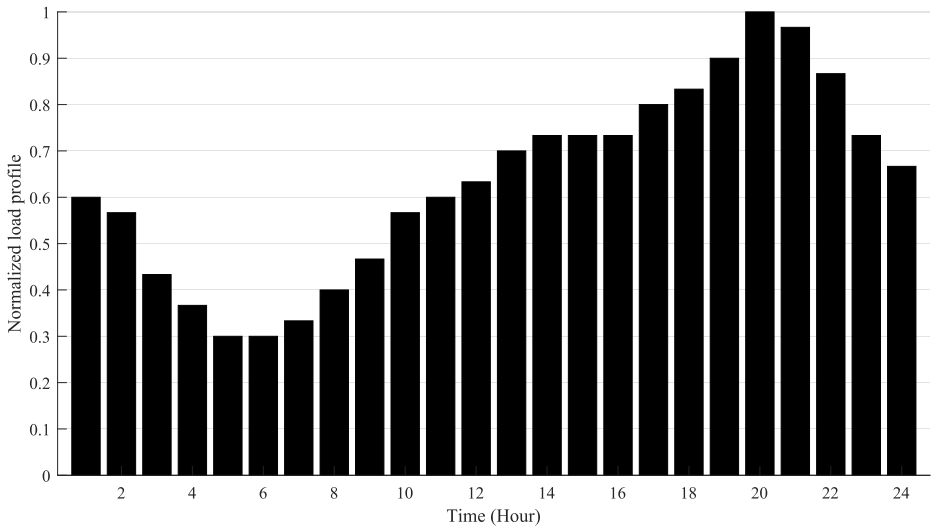

Fig. 7. The considered electricity load profile.

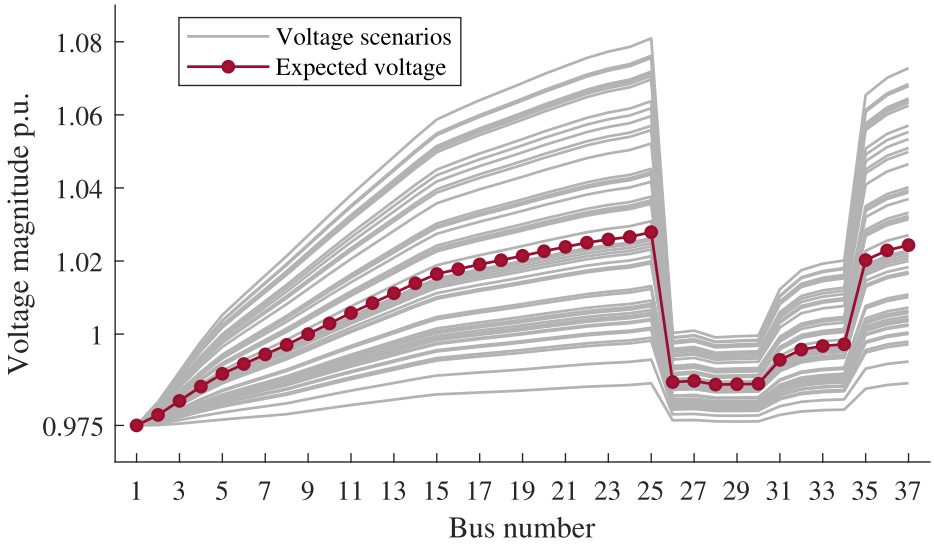

Fig. 8. Voltage profiles of the final set of scenarios in the first level of the proposed voltage control strategy.

and 25, according to the explained model in Section 3, start to absorb reactive power. Taking into account the new condition, an overall load flow is executed (second step in Fig. 3). The improved voltage profile after performing each iteration is shown in Fig. 10. Since the absorbed power capability of the inverters within partition P_5 are not enough, the voltage profile is still outside of the allowed range. For this reason, according to the algorithm presented in Fig. 3, steps 2 and 3 will be repeated again. In this level, since partition P_4 experiences the worst voltage magnitude, this partition will be selected to absorb reactive power. In the next steps, in this case, one additional partition will be involved at each time in the process of voltage control. This process will be continued until the voltage of any node in the grid does not exceed the allowed range.

Fig. 11 shows the amount of absorbed reactive power in each partition after finishing the process of voltage control. It should be noted that the explained procedure is for the highest PV generation time-period (hour 13). In hours with less PV production, there is a need for less number of partitions to participate in the process of reactive power voltage control. In this way, other inverters can continue their operation with power factor 1. Furthermore, in hours without PV production only level one of the proposed voltage control method is able to improve the voltage profile of the system.

The amount of improvement in the voltage profile of the network after adding each partition to the second level of the proposed voltage control strategy is depicted in Fig. 10. At first, partition P_5 and then partitions P_4 are considered respectively, to improve the voltage profile of the system in the second level of the proposed voltage control strategy.

Voltage profiles of buses for different cases, including the base case, installing PV units in candidate buses, voltage control using only the first level and the proposed two-level voltage control strategy is shown in Fig. 12. Moreover, in Fig. 13, bus 25 is selected as the most critical node in the system. Here, the results for the next 24 time-periods is depicted. As shown in these figures, the proposed voltage control strategy using OLTC and appropriate scheduling of the batteries in the first level and absorbing reactive power in the second level can keep the voltage within the permissible range.

In order to show the performance of the proposed voltage control method, the buses from different partitions of the system are selected. Table 2 illustrates the obtained results for these buses. In this table, the impact of batteries in the first level and RPC in the second level of the proposed methodology is presented. The represented data in this table is

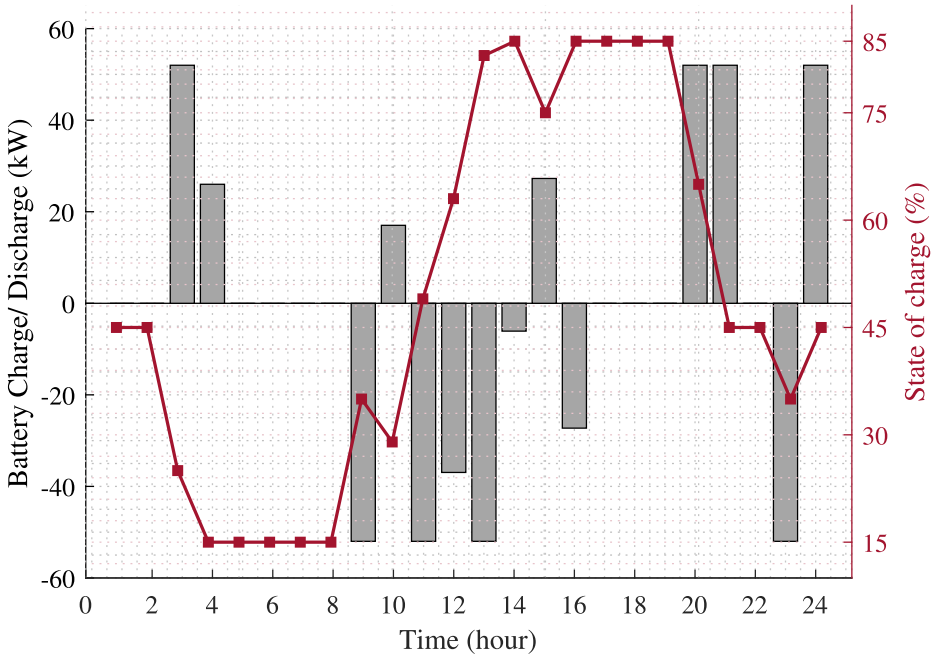

Fig. 9. Charge (negative values)/ discharge (positive values) rates of the battery and PV production in bus 35.

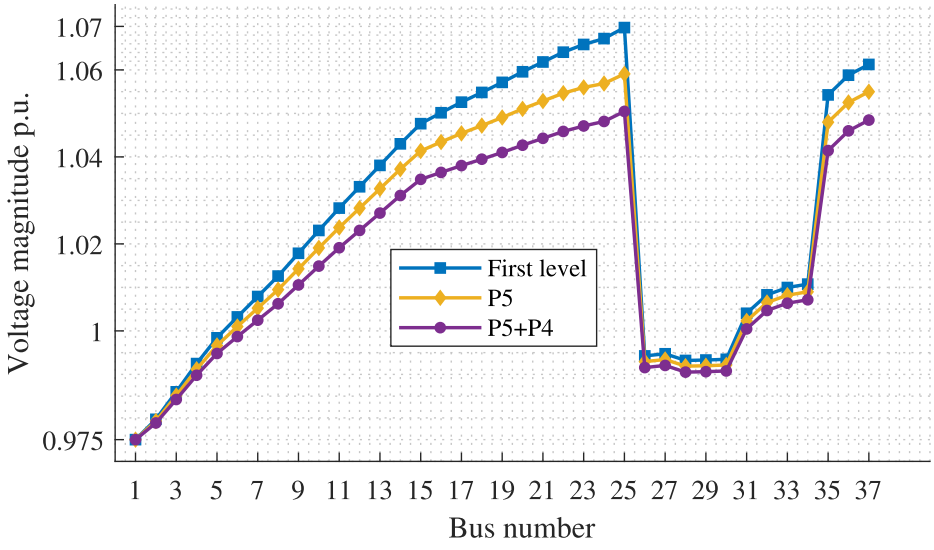

Fig. 10. Voltage profile after involving different partitions in level two in the time-period with the highest solar penetration (hour 13).

for the hour with the maximum amount of solar penetration (hour 13). In this time-period, the tap position of OLTC is located on level −4 and the voltage in the reference bus is 0.975. For instance, as can be seen in this table, in bus 25, the voltage magnitude before applying the proposed strategy is 1.083, which exceeds the bus voltage limitation. To this end the first level of the proposed method is implemented, which improves the voltage magnitude of this bus to 1.071. However, the obtained value is still not within the permissible range of voltage magnitude. Therefore the second level of the proposed method is applied, which decreases the voltage magnitude to 1.05 by absorption 429 kVar. Therefore, in the times with high PV production, using the proposed two-level voltage control is essential to keep the voltage within the permissible range.

For the sake of comparison, in Table 3, the simulation results for a different number of scenarios are expressed. For this purpose, the total amount of absorbed reactive power for the real day, as well as the time of the simulation are demonstrated. According to this table, by increasing the number of scenarios, the amount of absorbed reactive power slightly changes, whereas the simulation time increases significantly.

We compared the simulation results with the model presented in [30], which we believe is the closest to the proposed model. Although there are some differences, we managed to compare the specific hour in the model, where the PV production is similar to our case study. In [30], the simulation results for 1140^{th} hour in the year, in which, the PV production is 0.8295 p.u. is presented. The results show that for regulating voltages within the acceptable range, total amounts of 1302.48 kVar reactive power absorption and 2161.35 kW active power curtailment is needed. However, in our study for hour 13 with a 0.95 p.u. PV production the amount of absorbed reactive power is 1818.3 kVar, and no active power curtailment is needed.

All simulations in this article are executed using MATLAB-GAMS

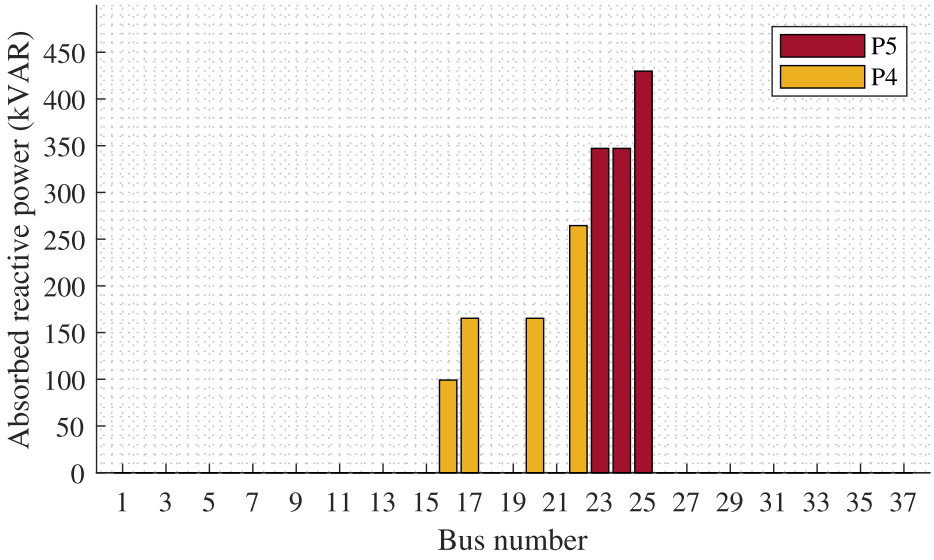

Fig. 11. The amount of absorbed reactive power in different partitions at hour 13.

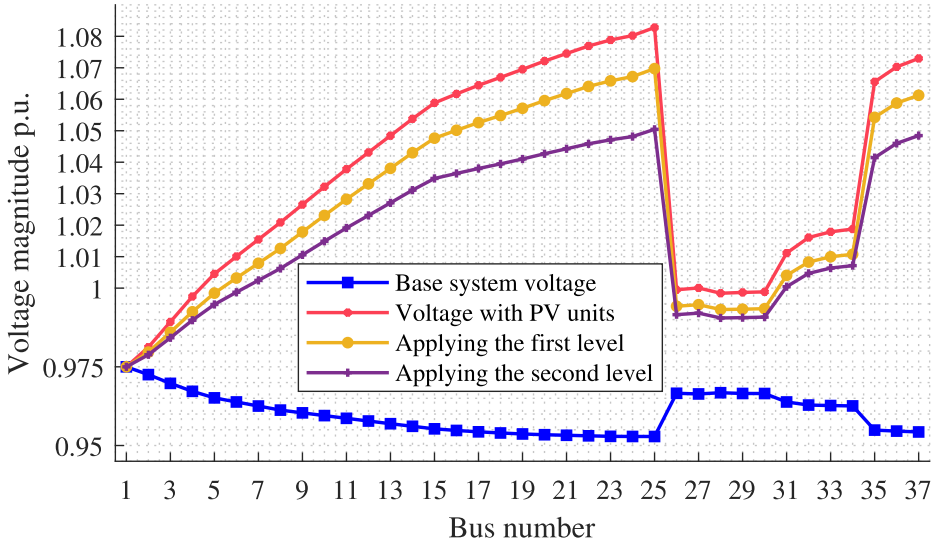

Fig. 12. Voltage profile for different modes in the time-period with the highest solar penetration.

interface. The network partitioning part is coded in MATLAB environment. Also, the applied optimisation models for the first and second levels of the proposed two-level voltage control strategy are modelled in the GAMS optimisation environment and solved by CPLEX solver on a laptop computer with i5 intel(R) core, 2.30 GHz CPU and 4 GB RAM.

The computational time for the proposed voltage control strategy is 273 and 10 s for the first and the second level, respectively. This running time is compatible for the day ahead optimisation.

5. Conclusion & future work

The over-voltage issue in low voltage distribution networks with high penetration of PVs is one of the most important challenges in the development of renewable resources in distribution grids. In this paper, a two-level voltage control methodology is proposed to deal with the over-voltage problem. In the first level, a stochastic optimisation model is proposed to set the OLTC tap position and schedule the operation of batteries in a way that the voltage profile improves. Based on generated scenarios for PV production, the optimal charging and discharging schedule of the batteries for the next 24 time-periods will be done in a way that, the bus voltages are kept as close as possible to the rated values. In the second level, based on the partitioning of the distribution grid, an optimisation model is proposed to use RPC capability of PV inverters. By applying the proposed strategy, the capability of inverters located in the most critical partitions will be optimally used for reactive power consumption. The proposed voltage control strategy benefits from OLTC, battery scheduling and RPC capability of inverters for the horizons of one-day and one-hour ahead, respectively; and it has the advantages of all mentioned methods at the same time. Compared with other RPC strategies, due to selecting the most critical partitions, the number of control buses are less, and the amount of absorbed reactive power is well optimized among them.

The future works of this study can be directed to assessment of the capability of the proposed method under different conditions considering stochastic behaviours of solar generation, wind generation [45] and demand of consumers. Also, in the current model, the single-phase balanced equivalent model is considered to simulate the distribution network. The unbalanced network will be considered in future work.

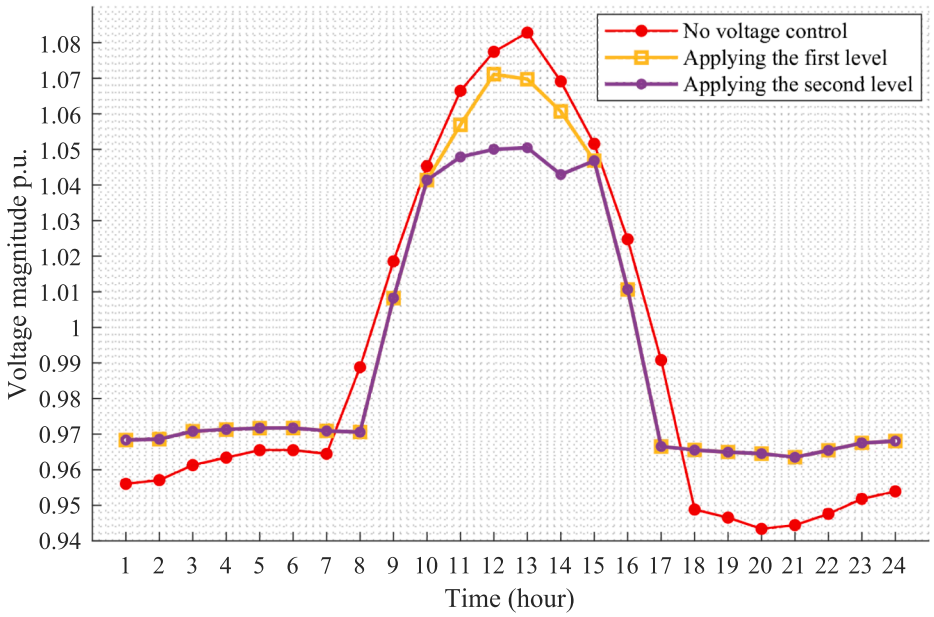

Fig. 13. Voltage profile of the bus 25 for the next 24 time-periods.

Table 2
Characteristics of different buses before and after applying the first and second level of the proposed strategy.

Bus number	Characteristics before applying voltage control				Characteristics after applying the first level		Characteristics after applying the second level	
	P (kW)	Q (kVar)	PV (kW)	V (p.u.)	Battery charging (kW)	V (p.u.)	Q absorption (kVar)	V (p.u.)
2	377	81	1000	0.981	40	0.978	0	0.0978
8	491	156	250	1.021	10	1.013	0	1.006
20	80	32	500	1.072	20	1.060	165	1.043
25	2	2	1300	1.083	52	1.071	429	1.050
32	357	119	2000	1.016	78	1.008	0	1.005
37	110	65	1500	1.073	38	1.061	0	1.048

Table 3
Total amount of RPC and simulation time for a different number of scenarios.

Number of Scenarios	Q absorption (kVar)	Time (Sec)
5	4836.9	24
25	4684.4	134
50	3840.1	283
100	3444.5	751
200	3444.5	1502

CRediT authorship contribution statement

Mohammadreza Emarati: Conceptualization, Data curation, Formal analysis, Formal analysis, Investigation, Methodology, Software, Validation, Writing - original draft. **Mostafa Barani:** Conceptualization, Data curation, Investigation, Methodology, Software, Validation, Writing - original draft. **Hossein Farahmand:** Conceptualization, Data curation, Formal analysis, Investigation, Methodology, Supervision, Validation, Writing - review & editing. **Jamshid Aghaei:** Conceptualization, Data curation, Formal analysis, Methodology, Supervision, Validation, Writing - review & editing. **Pedro Crespo Del Granado:** Conceptualization, Formal analysis, Supervision, Validation, Writing - review & editing.

Declaration of Competing Interest

The authors declare that they have no known competing financial interests or personal relationships that could have appeared to influence the work reported in this paper.

***

***

Appendix A

As illustrated in Fig. 2. Linearisation of inverter capability curve is performed by dividing its operation range into two different modes: heavy load and light load. Operation mode in heavy load times is depicted in Fig. 2 (a). Due to the high consumption, the battery and PV sets primarily produce active power and then in the next level the reactive power control capability is applied. In this case, lines l_1 and l_2 limit the inverter to remain in the heavy load operating range. Also, the constraints about reactive power are applied by lines l_3 and l_4.

$$l_1 = P_g - \left(\frac{S_{\text{inv}} - P(Q_{\max})}{-Q_{\max}}\right) \times Q_g - S_{\text{inv}} \tag{31}$$

$$l_2 = P_g - \left(\frac{S_{\text{inv}} - P(-Q_{\max})}{Q_{\max}}\right) \times Q_g - S_{\text{inv}} \tag{32}$$

$$l_3 = Q + Q_{\max} \tag{33}$$

$$l_4 = Q - Q_{\max} \tag{34}$$

In light-load mode, the battery works as an auxiliary service, with less emphasis on active power injection into the network. So, as it shown in Fig. 2 (b) the power exchange between DGs and the grid is limited in a predefined range. The lines l_5 to l_{10} in this figure describe the operational constraints for the inverter in light-load conditions.

$$l_5 = P_g - \left(\frac{P_{\max}}{S_{\text{inv}} - Q(P_{\max})}\right) \times Q_g - \left(\frac{P_{\max}}{S_{\text{inv}} - Q(P_{\max})}\right) \times S_{\text{inv}} \tag{35}$$

$$l_6 = P_g + \left(\frac{P_{\max}}{S_{\text{inv}} - Q(P_{\max})}\right) \times Q_g + \left(\frac{P_{\max}}{S_{\text{inv}} - Q(P_{\max})}\right) \times S_{\text{inv}} \tag{36}$$

$$l_7 = P_g + \left(\frac{P_{\max}}{S_{\text{inv}} - Q(P_{\max})}\right) \times Q_g - \left(\frac{P_{\max}}{S_{\text{inv}} - Q(P_{\max})}\right) \times S_{\text{inv}} \tag{37}$$

$$l_8 = P_g - \left(\frac{P_{\max}}{S_{\text{inv}} - Q(P_{\max})}\right) \times Q_g + \left(\frac{P_{\max}}{S_{\text{inv}} - Q(P_{\max})}\right) \times S_{\text{inv}} \tag{38}$$

$$l_9 = P_g - P_{\max} \tag{39}$$

$$l_{10} = P_g + P_{\max} \tag{40}$$

Appendix B. Supplementary material

Supplementary data associated with this article can be found, in the online version, at https://doi.org/10.1016/j.ijepes.2021.106763.

References

[1] Zervos A, Lins C. Renewables 2016 Global Status Report, Council of the Federation; 2016.

[2] Molina-García A, Mastromauro RA, García-Sánchez T, Pugliese S, Liserre M, Stasi S. Reactive power flow control for PV inverters voltage support in lv distribution networks. IEEE Trans Smart Grid 2017;8(1):447–56.

[3] R. Energy, Accelerating the global energy transformation, International Renewable Energy Agency (IRENA). Abu Dhabi; 2017.

[4] Yang H-T, Chen Y-T, Liao J-T, Yang C-T. Over-voltage mitigation control strategies for distribution system with high PV penetration, in. In: 2015 18th international conference on Intelligent System Application to Power Systems (ISAP), IEEE; 2015. p. 1–6.

[5] Mokhtari G, Ghosh A, Nourbakhsh G, Ledwich G. Smart robust resources control in LV network to deal with voltage rise issue. IEEE Trans Sustain Energy 2013;4(4):1043–50.

[6] Wang Y, Xu Y, Tang Y, Syed MH, Guillo-Sansano E, Burt GM. Decentralised-distributed hybrid voltage regulation of power distribution networks based on power inverters. IET Gen Transm Distrib 2018;13(3):444–51.

[7] Liu X, Aichhorn A, Liu L, Li H. Coordinated control of distributed energy storage system with tap changer transformers for voltage rise mitigation under high photovoltaic penetration. IEEE Trans Smart Grid 2012;3(2):897–906.

[8] Forte de Oliveira Luna JD, Renato da Costa Mendes P, Normey-Rico JE. A convex optimal voltage unbalance compensator for hybrid AC/DC microgrids. In: 2019 IEEE PES innovative smart grid technologies conference - Latin America (ISGT Latin America); 2019. p. 1–6. doi:10.1109/ISGT-LA.2019.8895461.

[9] Mokhtari G, Nourbakhsh G, Ledwich G, Ghosh A. Overvoltage and overloading prevention using coordinated PV inverters in distribution network, in. In: Industrial electronics society, IECON 2014–40th Annual Conference of the IEEE, IEEE; 2014. p. 5571–4.

[10] Tonkoski R, Lopes LA, El-Fouly TH. Coordinated active power curtailment of grid connected PV inverters for overvoltage prevention. IEEE Trans Sustain Energy 2011;2(2):139–47.

[11] Wang S, Chen S, Ge L, Wu L. Distributed generation hosting capacity evaluation for distribution systems considering the robust optimal operation of OLTC and SVC. IEEE Trans Sustain Energy 2016;7(3):1111–23.

[12] Kim B, Nam Y-H, Ko H, Park C-H, Kim H-C, Ryu K-S, Kim D-J. Novel voltage control method of the primary feeder by the energy storage system and step voltage regulator. Energies 2019;12(17):3357.

[13] Homaee O, Zakariazadeh A, Jadid S. Real-time voltage control algorithm with switched capacitors in smart distribution system in presence of renewable generations. Int J Electrical Power Energy Syst 2014;54:187–97.

[14] Ghosh S, Rahman S, Pipattanasomporn M. Distribution voltage regulation through active power curtailment with PV inverters and solar generation forecasts. IEEE Trans Sustain Energy 2017;8(1):13–22.

[15] Wu L, Guan L. Integer quadratic programming model for dynamic VAR compensation considering short-term voltage stability. IET Gen Transm Distrib 2018;13(5):652–61.

[16] Kontis EO, Kryonidis GC, Nousdilis AI, Malamaki K-ND, Papagiannis GK. A two-layer control strategy for voltage regulation of active unbalanced LV distribution networks. Int J Electrical Power Energy Syst 2019;111:216–30.

[17] Wang Y, Zhao T, Ju C, Xu Y, Wang P. Two-level distributed voltage/var control using aggregated pv inverters in distribution networks. IEEE Trans Power Delivery; 2019.

[18] Wang Y, Syed MH, Guillo-Sansano E, Xu Y, Burt GM. Inverter-based voltage control of distribution networks: a three-level coordinated method and power hardware-in-the-loop validation. IEEE Trans Sustain Energy.

[19] Salih SN, Chen P. On coordinated control of OLTC and reactive power compensation for voltage regulation in distribution systems with wind power. IEEE Trans Power Syst 2016;31(5):4026–35.

[20] Tina GM, Garozzo D, Siano P. Scheduling of PV inverter reactive power set-point and battery charge/discharge profile for voltage regulation in low voltage networks. Int J Electrical Power Energy Syst 2019;107:131–9.

[21] Zhang D, Li J, Hui D. Coordinated control for voltage regulation of distribution network voltage regulation by distributed energy storage systems. Protect Control Mod Power Syst 2018;3(1):3.

[22] von Appen J, Stetz T, Braun M, Schmiegel A. Local voltage control strategies for PV storage systems in distribution grids. IEEE Trans Smart Grid 2014;5(2):1002–9.

[23] Wang L, Bai F, Yan R, Saha TK. Real-time coordinated voltage control of PV inverters and energy storage for weak networks with high PV penetration. IEEE Trans Power Syst 2018;33(3):3383–95.

[24] Zhang Y, Meng K, Luo F, Yang H, Zhu J, Dong ZY. Multi-agent-based voltage regulation scheme for high photovoltaic penetrated active distribution networks using battery energy storage systems. IEEE Access 2019;8:7323–33.

[25] Zhang C, Chu X. Voltage regulation strategy for active distribution network coordinating DGs, ESS units and OLTC. In: 2017 IEEE power & energy society general meeting, IEEE; 2017. p. 1–5.

[26] Gao H, Liu J, Wang L. Robust coordinated optimization of active and reactive power in active distribution systems. IEEE Trans Smart Grid 2017;9(5):4436–47.

[27] Hashemi S, Østergaard J. Methods and strategies for overvoltage prevention in low voltage distribution systems with PV. IET Renew Power Gener 2016;11(2):205–14.

[28] Cheng Z, Li Z, Liang J, Si J, Dong L, Gao J. Distributed coordination control strategy for multiple residential solar PV systems in distribution networks. Int J Electrical Power Energy Syst 2020;117:105660.

[29] Hu X, He W, Li L, Lin Y, Li H, Pan J. An efficient and fast algorithm for community detection based on node role analysis. Int J Mach Learn Cybernet 2019;10(4):641–54.
[30] Zhao B, Xu Z, Xu C, Wang C, Lin F. Network partition-based zonal voltage control for distribution networks with distributed PV systems. IEEE Trans Smart Grid 2018;9(5):4087–98.
[31] Barani M, Aghaei J, Akbari MA, Niknam T, Farahmand H, Korpås M. Optimal partitioning of smart distribution systems into supply-sufficient microgrids. IEEE Trans Smart Grid 2019;10(3):2523–33.
[32] Kundu S, Backhaus S, Hiskens IA. Distributed control of reactive power from photovoltaic inverters, in. In: 2013 IEEE International Symposium on Circuits and Systems (ISCAS), IEEE; 2013. p. 249–52.
[33] Nayeripour M, Fallahzadeh-Abarghouei H, Waffenschmidt E, Hasanvand S. Coordinated online voltage management of distributed generation using network partitioning. Electric Power Syst Res 2016;141:202–9.
[34] Girvan M, Newman ME. Community structure in social and biological networks. Proc Natl Acad Sci 2002;99(12):7821–6.
[35] Li P, Zhang C, Wu Z, Xu Y, Hu M, Dong Z. Distributed adaptive robust voltage/var control with network partition in active distribution networks. IEEE Trans Smart Grid 2020;11(3):2245–56.
[36] Stetz T, Marten F, Braun M. Improved low voltage grid-integration of photovoltaic systems in Germany. IEEE Trans Sustain Energy 2013;4(2):534–42.
[37] Bayer B, Matschoss P, Thomas H, Marian A. The German experience with integrating photovoltaic systems into the low-voltage grids. Renewable Energy 2018;119:129–41.
[38] Agalgaonkar YP, Pal BC, Jabr RA. Distribution voltage control considering the impact of PV generation on tap changers and autonomous regulators. IEEE Trans Power Syst 2014;29(1):182–92.
[39] Bozorgavari SA, Aghaei J, Pirouzi S, Nikoobakht A, Farahmand H, Korpås M. Robust planning of distributed battery energy storage systems in flexible smart distribution networks: A comprehensive study. Renew Sustain Energy Rev 2020;123:109739.
[40] Atwa YM, El-Saadany E. Optimal allocation of ess in distribution systems with a high penetration of wind energy. IEEE Trans Power Syst 2010;25(4):1815–22.
[41] Robert C, Casella G. Monte Carlo statistical methods. Springer Science & Business Media; 2013.
[42] Conejo AJ, Carrión M, Morales JM, et al. Decision making under uncertainty in electricity markets, vol. 1. Springer; 2010.
[43] IEEE guide for design, operation, and integration of distributed resource island systems with electric power systems, IEEE Std 1547.4-2011 (2011) 1–54. doi: 10.1109/IEEESTD.2011.5960751.
[44] Advancing Reanalysis; 2019, https://reanalyses.org/.
[45] Del Granado PC, Wallace SW, Pang Z. The impact of wind uncertainty on the strategic valuation of distributed electricity storage. CMS 2016;13(1):5–27.